Inorganic Chemistry

pubs.acs.org/IC Article

Energy Migration Processes in Re(I) MLCT Complexes Featuring a Chromophoric Ancillary Ligand

Kaylee A. Wells, James E. Yarnell, Jonathan R. Palmer, Tia S. Lee, Christopher M. Papa, and Felix N. Castellano*

Cite This: *Inorg. Chem.* 2020, 59, 8259–8271 Read Online

ACCESS | Metrics & More | Article Recommendations | Supporting Information

ABSTRACT: We present the synthesis, structural characterization, electronic structure calculations, and ultrafast and supra-nanosecond photophysical properties of a series of five Re(I) bichromophores exhibiting metal to ligand charge transfer (MLCT) excited states based on the general formula *fac*-[Re(N^N)(CO)$_3$(PNI-py)]PF$_6$, where PNI-py is 4-piperidinyl-1,8-naphthalimidepyridine and N^N is a diimine ligand (**Re1−5**), along with their corresponding model chromophores where 4-ethylpyridine was substituted for PNI-py (**Mod1−5**). The diimine ligands used include 1,10-phenanthroline (phen, **1**), 2,9-dimethyl-4,7-diphenyl-1,10-phenanthroline (bcp, **2**), 4,4′-di-*tert*-butyl-2,2′-bipyridine (dtbb, **3**), 4,4′-diethyl ester-2,2′-bipyridine (deeb, **4**), and 2,2′-biquinoline (biq, **5**). In these metal−organic bichromophores, structural modification of the diimine ligand resulted in substantial changes to the observed energy transfer efficiencies between the two chromophores as a result of the variation in ^{3}MLCT excited-state energies. The photophysical properties and energetic pathways of the model chromophores were investigated in parallel to accurately track the changes that arose from introduction of the organic chromophore pendant on the ancillary ligand. All relevant photophysical and energy transfer processes were probed and characterized using time-resolved photoluminescence spectroscopy, ultrafast and nanosecond transient absorption spectroscopy, and time-dependent density functional theory calculations. Of the five bichromophores in this study, four (**Re1−4**) exhibited a thermal equilibrium between the ^{3}PNI-py and the ^{3}MLCT excited state, drastically extending the lifetimes of the parent model chromophores.

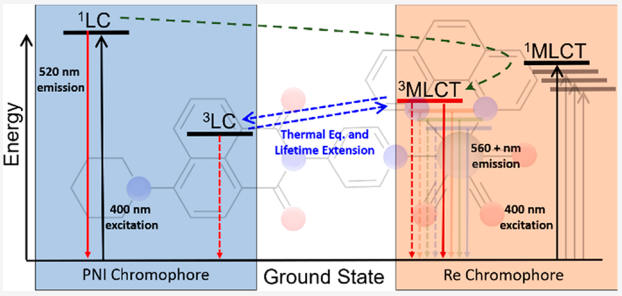

INTRODUCTION

Rhenium(I) carbonyl diimine (Re-CDI) complexes of the generic form *fac*-[Re(N^N)(CO)$_3$(L)]$^+$ (where N^N is a bidentate diimine ligand and L is a neutral ligand or anion) have been of interest to researchers since the first publication by Wrighton and co-workers in the 1970s due to their diverse photophysical behavior.[1] These molecules are thermally and photochemically stable, exhibit expansive photophysical tunability, and are relatively easy to synthesize.[2] Since Wrighton and co-workers first reported a comprehensive investigation into Re(I)-CDI complexes, these molecules have become pivotal to the study of excited-state electron transfer (ET) and energy transfer (EnT) processes. Applications that utilize such excited-state chemistry include photochemical molecular devices, solar energy conversion, photovoltaics, chemical sensing, photoredox catalysis, and biotechnology applications such as DNA intercalation, along with many others.[3−11]

The myriad applications of Re-CDI complexes directly results from their low-energy, visible absorption bands and their long-lived, solvent-sensitive, lowest energy triplet metal to ligand charge transfer (MLCT) excited states that are strongly photoluminescent.[2,3,5,8] The structure of these molecules enables facile synthetic manipulation of the diimine or ancillary ligands, resulting in deterministic changes to the triplet MLCT photoluminescence (PL). Variation of the ancillary ligand modulates the energy levels of the Re(I) dπ orbitals and therefore the HOMO energies.[1,12,13] In contrast, modification of the diimine ligand affects the first reduction potential of the Re-CDI, altering the charge transfer energy via changes in the LUMO energy. When the HOMO and LUMO gap is changed through ligand modification, the MLCT energy correspondingly changes.[1,12,13] Moreover, extension of the π conjugation or addition of an organic chromophore to either the diimine ligand or ancillary ligand generates ligand-centered (LC) excited states in these molecules. Strategic adjustments in the ligand moieties can increase the visible absorption cross sections and may rigidify the molecular framework to decrease nonradiative decay in the resultant metal complexes which

Received: February 28, 2020
Published: June 3, 2020

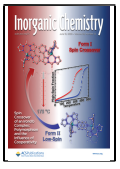

https://dx.doi.org/10.1021/acs.inorgchem.0c00644
Inorg. Chem. 2020, 59, 8259−8271

improves their effectiveness toward ET and EnT processes. Previously, reversible energy transfer at room temperature has been reported when energetically proximate inorganic and organic chromophores were fused together in the same transition metal complex.[14] These polychromophoric systems can be designed to access synergetic properties of the composite chromophores, including lifetime extension, which is imperative to many applications for a number of research groups,[14−25] including our own.[26−31]

We have extensively investigated the intriguing photophysical properties that arise after linking 4-piperidinylnaphthalimide (PNI) and other naphthalimide (NI) derivatives to transition-metal complexes.[4,32−34] In 2011, Yarnell and coworkers demonstrated that, when PNI was covalently linked to the 5-position of 1,10-phenanthroline on a Re-CDI, the molecule exhibited "ping-pong" energy transfer between the MLCT and PNI excited states (Figure 1). In that study, time-

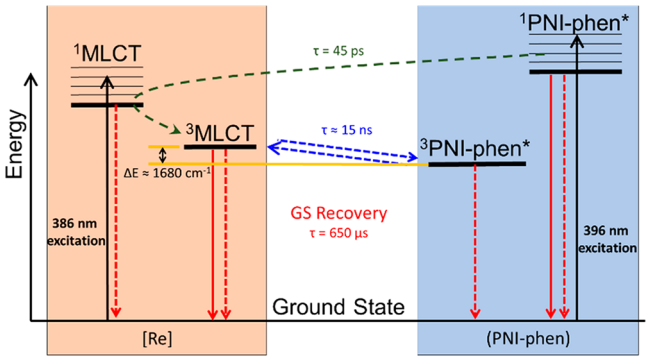

Figure 1. Qualitative energy level diagram describing the "ping-pong" energy transfer process between the Re(I) MLCT and PNI excited states.[4]

resolved PL and transient absorption (TA) spectroscopy from the subpicosecond to the microsecond time domain were utilized to monitor the excited-state dynamics of the complex. These spectroscopic measurements revealed energy transfer from ^{1}PNI to the ^{1}MLCT excited state through Förster resonance energy transfer (FRET) featuring a time constant of 43 ps, ultimately yielding the ^{3}MLCT excited state. Furthermore, the ^{3}MLCT state participated in back energy transfer (reverse triplet−triplet energy transfer, rTTET) to the triplet manifold of the PNI subunit within 20 ns through a Dexter-like process. Due to the energetic proximity (ΔE = 1680 cm^{-1}) and the rapid rate of energy transfer occurring between the two triplet excited states, the thermal equilibrium process extended the excited-state lifetime of the parent Re-CDI from 197 ns to 651 μs.[4]

Although this initial study established the precedence for lifetime extension and increased visible absorption cross sections resulting from the fusion of inorganic and organic chromophores, there were a few remaining questions that could not be addressed. If low fluorescence quantum yield organic chromophores were used instead of the highly emissive PNI chromophore, could singlet energy transfer still occur? Additionally, what energy gap between the ^{3}MLCT and ^{3}LC excited states is sufficient for rTTET to occur effectively at room temperature? To address these concerns, we studied the effects of five weakly emissive NIs on the rate of FRET from NI to Re-CDI while investigating the effects of varying the energy levels of the NI fragment on the resulting thermal equilibrium between the NI and Re-CDI subunits. In these instances, four of the five bichromophores studied still exhibited "ping-pong" energy transfer behavior.[31]

While we have examined the influence of NI donor ligands on the resultant energy transfer processes, the influence of the MLCT energetics on these processes has never been addressed. In particular, what happens when the MLCT energy levels are altered without changing those of the ligand-centered excited state? To significantly modify the energy levels of the MLCT excited states in Re-CDI complexes, the diimine ligand must be changed; therefore, the previous approach where the NI subunit was covalently linked to the backbone of 1,10-phenanthroline can no longer be used. Instead the PNI chromophore for the current series was appended onto the Re(I) core through the 4-position of the ancillary pyridine ligand, freeing up the diimine ligand for systematic alteration. Here, five newly conceived Re(I) bichromophores, *fac*-[Re(phen)(CO)$_3$(PNI-py)](PF$_6$) (phen = 1,10-phenanthroline, **1**), *fac*-[Re(bcp)(CO)$_3$(PNI-py)](PF$_6$) (bcp = 2,9-dimethyl-4,7-diphenyl-1,10-phenanthroline, **2**), *fac*-[Re(dtbb)(CO)$_3$(PNI-py)](PF$_6$) (dtbb = 4,4′-di-*tert*-butyl-2,2′-bipyridine, **3**), *fac*-[Re(deeb)(CO)$_3$(PNI-py)](PF$_6$) (deeb = 4,4′-diethyl ester-2,2′-bipyridine, **4**), and *fac*-[Re(biq)(CO)$_3$(PNI-py)](PF$_6$) (biq = 2,2′-biquinoline, **5**) (**Re1−5**, respectively) along with five Re(I) model MLCT chromophores, *fac*-[Re(N^N)(CO)$_3$(4-etpy)](PF$_6$) (where N^N = phen, bcp, dtbb, deeb, biq and 4-etpy is 4-ethylpyridine), (**Mod1−5**, respectively; Figure 2) were synthesized and investigated using steady-state and time-

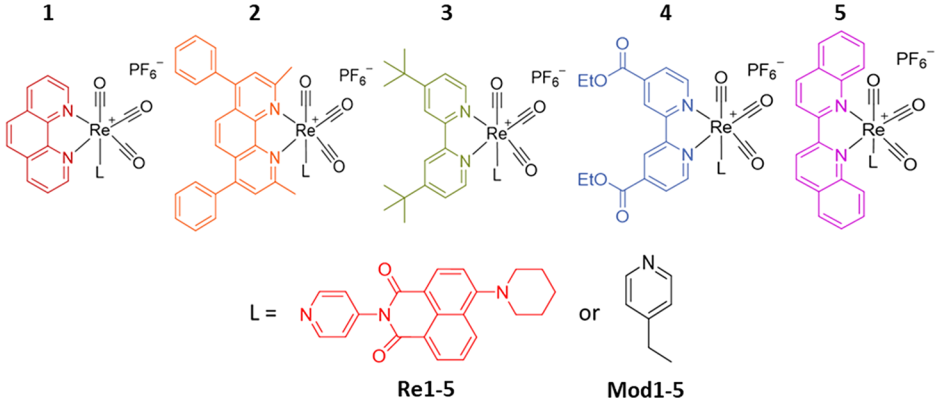

Figure 2. Re(I) chromophores and Re(I)-PNI bichromophores investigated in this study.

https://dx.doi.org/10.1021/acs.inorgchem.0c00644
Inorg. Chem. 2020, 59, 8259−8271

resolved PL and electronic spectroscopy as well as computational modeling to determine the effects of varying the MLCT energy levels on the energy transfer processes in the Re(I) bichromophores. It is interesting to note that, in addition to determining what energy gaps are necessary to enable the various energy transfer processes in **Re1−5**, the proposed architecture of these bichromophores enables examination of the effect of the physical separation between the two constituents on the rate of respective photophysical processes and whether these processes can be partially or completely attenuated in the spatial separation achieved across these conserved molecular geometries.

EXPERIMENTAL SECTION

Reagents and Chemicals. All syntheses were performed under an inert, dry nitrogen atmosphere using standard techniques. All reagents were purchased from Sigma-Aldrich or Alfa Aesar and used as received. Spectroscopic samples were prepared using spectroscopic-grade tetrahydrofuran and were degassed using the freeze−pump−thaw technique for at least four cycles. The diimine ligand deeb was synthesized according to literature procedures and used without any additional purification.[35] Complete synthesis and structural characterization details for all molecules investigated here are provided as Supporting Information.

General Techniques. ^{1}H NMR spectra were recorded with a Varian Innova 400 instrument operating at a working frequency of 400 MHz. Electronic absorption spectra were measured with a Shimadzu UV-3600 and Cary 60 UV/vis spectrophotometer. Steady-state photoluminescence spectra were measured on an Edinburgh FLS 980 or an Edinburgh FS920 fluorimeter. Quantum yield measurements were performed using degassed samples with $[Ru(bpy)_3](PF_6)_2$ in acetonitrile as a standard (λ_{em} 621 nm, Φ_p = 0.095)[36] for both the PNI-py and model complexes. The PNI-py complexes (**Re1−5**) were referenced to an additional standard, PNI in toluene (λ_{em} 498 nm, Φ_f = 0.91).[37] Attenuated total reflectance Fourier-transform infrared (ATR-FTIR) spectroscopy on solid samples was conducted using a Bruker Alpha Platinum ATR instrument. High-resolution electrospray mass spectrometry was carried out by the Michigan State University Mass Spectrometry Core, East Lansing, MI. Elemental analyses were determined by Atlantic Microlab, Inc., Norcross, GA.

Electrochemistry. Differential-pulse voltammetry (DPV) measurements were performed using a CH Instruments Model 600E series potentiostat. The measurements were carried out under an inert and dry atmosphere of nitrogen in a glovebox (MBraun). Reduction potentials were recorded in tetrahydrofuran containing 0.1 M tetrabutylammonium hexafluorophosphate ($TBAPF_6$) as the supporting electrolyte. A platinum disk was used as the working electrode (1.6 mm), a platinum wire as the counter electrode, and $Ag/AgNO_3$ as the reference electrode.

Femtosecond Transient Absorption Spectroscopy. The transient absorption measurements were performed at the NCSU Imaging and Kinetic Spectroscopy (IMAKS) Laboratory using a mode-locked Ti:sapphire laser (Coherent Libra) as described previously.[38] The pump beam was directed into a parametric amplifier (Coherent OPerA Solo) to generate the 400 nm excitation. The probe beam was focused onto a calcium fluoride crystal to generate a white light continuum between 350 and 775 nm. The pump beam (~700 μm) was focused and overlapped with the probe beam through a 2 mm path length cuvette to allow for a stir bar to be used. The ground-state absorption spectra were taken before and after each experiment to ensure there was no sample photodegradation during the experiment. The transient kinetic data at specific wavelengths was evaluated using the fitting routines available in OriginPro 2018b (v 9.55).

Nanosecond Transient Absorption Spectroscopy. Nanosecond transient absorption measurements were collected with a LP920 laser flash photolysis system from Edinburgh Instruments. A Vibrant 355 Nd:YAG/OPO system (OPOTEK) was used for pulsed laser excitation for single wavelength kinetics. A Continuum Minilite Nd:YAG laser with 355 nm excitation was used to obtain the transient absorption difference spectra. To collect the transient absorption difference spectra in the visible portion of the spectrum, an iStar ICCD camera (Andor Technology) controlled by the LP920 software program was used. Samples were degassed using the freeze−pump−thaw technique for at least four cycles in a 10 mm path length quartz optical cell. Samples were prepared to have optical densities between 0.2 and 0.8 at the excitation wavelength (λ_{ex} 355 nm for difference spectra and λ_{ex} 410 nm for single-wavelength kinetics). All flash-photolysis experiments were performed at room temperature unless otherwise noted. The reported difference spectra and kinetic data are the average of 100 laser pulses. The ground-state electronic absorption spectra were recorded before and after each experiment to ensure no sample photodegradation. The transient kinetic data were evaluated using the fitting routines available in Origin Student 2018b (v. 9.55).

Time-Resolved Photoluminescence (TR-PL) Intensity Decay Measurements. Single-wavelength photoluminescence emission intensity decays for the model complexes (**Mod1−5**) and **Re5** were acquired with an LP920 laser flash photolysis system (Edinburgh Instruments) using the Vibrant 355 Nd:YAG/OPO system (OPOTEK) as the excitation source (λ_{ex} 410 nm). Photoluminescence decays were collected at their respective emission maxima. Time-gated emission spectra were collected using the same apparatus, except the 355 nm Minilite Nd:YAG laser was used for the excitation source instead. Emission spectra were collected using an iStar ICCD camera (Andor Technology), controlled by the LP920 software program. The reported time-gated emission spectra are the average of 100 laser pulses. For **Re1−4**, the single-wavelength emission intensity decays could not be obtained using the LP920 laser flash photolysis system or a nitrogen-pumped broad-band dye laser (2−3 nm fwhm) from PTI (GL-3300 N_2 laser, GL-301 dye laser), using an apparatus that has been previously described.[26] Due to the significant amount of unquenched fluorescence from the PNI-py ligand, reliable decays of the phosphorescence could not be recorded even when the red edge of the MLCT emission band was probed and are therefore not reported in this study.

Density Functional Theory (DFT) Calculations. The calculations utilized in this work were performed using the Gaussian 16 software package (Revision A.03)[39] and the computational resources of the North Carolina State University High Performance Computing Center. Ground-state and lowest energy triplet-state geometry optimizations were performed using the M06 functional,[40] along with the Def2-SVP basis set of the Alrichs group as implemented in Gaussian 16 for all nonmetal atoms.[41] The Stuttgart−Dresden effective core potentials (ECP) were used to replace the core electrons in rhenium for all calculations.[42] An f-polarization function was also added to the rhenium.[43] The polarizable continuum model (PCM) was used to simulate the tetrahydrofuran solvent environment for all calculations except the ground state geometry optimizations, in which the optimization was performed under vacuum followed by a single-point energy calculation with the PCM correction.[44] Frequency calculations were performed on all optimized structures, and no imaginary frequencies were found. An ultrafine grid was used in all calculations. The molecular orbitals involved in the low-lying singlet transitions as well as the triplet spin density surfaces were generated using GaussView 6.0.[45]

Time-Dependent DFT (TD-DFT) Calculations. Time-dependent calculations were performed on each respective optimized ground-state geometry using the Gaussian 16 software package (Revision A.03)[39,46−48] and the computation resources of the North Carolina State University High Performance Computing Center. The calculations were performed using the same level of theory as in the DFT calculations described above. The polarizable continuum model (PCM) correction was used to simulate the tetrahydrofuran solvent environment for all calculations.[44] The energy and oscillator strength were computed for each of the 50 lowest singlet excitations. The UV/

https://dx.doi.org/10.1021/acs.inorgchem.0c00644
Inorg. Chem. 2020, 59, 8259−8271

Scheme 1. Synthesis of PNI-py, the Re1−5 Bichromophores, and the Mod1−5 Model Chromophores[49,50]

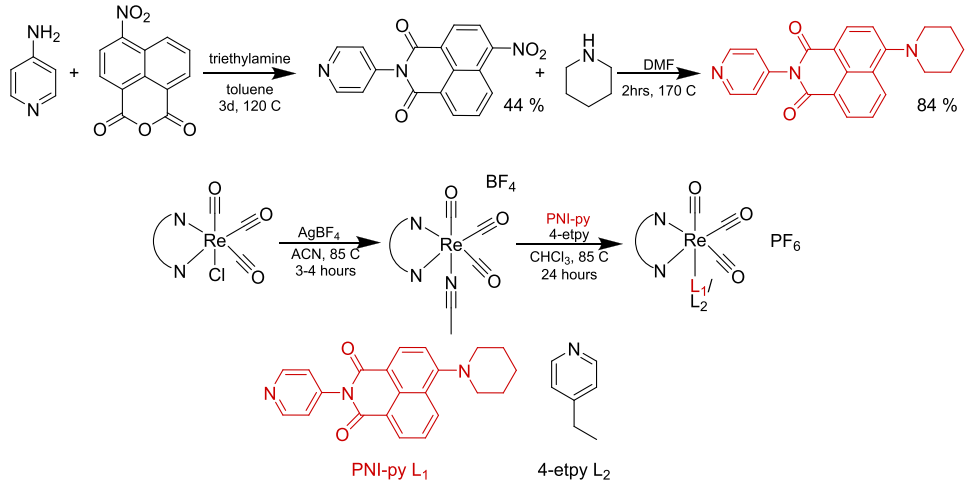

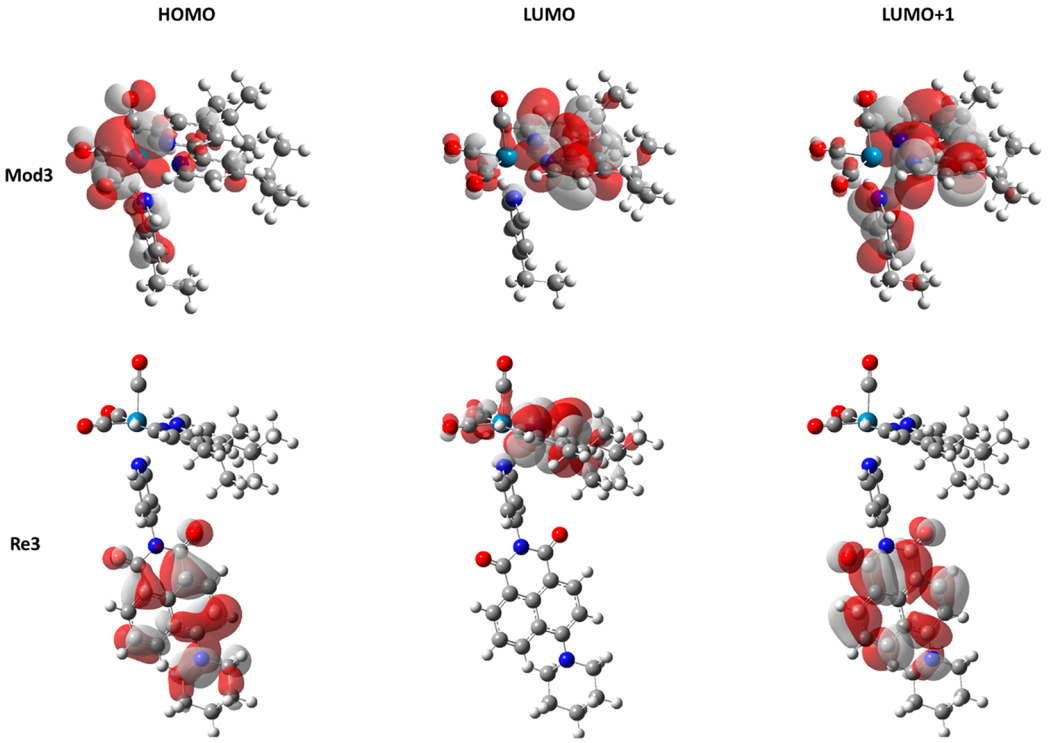

Figure 3. Representative schematic diagram of the HOMO, LUMO, and LUMO+1 of the model complexes (**Mod3** above) and rhenium bichromophores (**Re3** below).

vis spectra were generated from the singlet excitations using GaussView 6.0.[45]

RESULTS AND DISCUSSION

Synthesis. The PNI-py ligand and *fac*-[Re(N^N)-$(CO)_3$(PNI-py)](PF_6) (**Re1−5**) and *fac*-[Re(N^N)$(CO)_3$(4-etpy)](PF_6) (**Mod1−5**) (where N^N = phen (**1**), bcp (**2**), dtbb (**3**), deeb (**4**), biq (**5**)) were synthesized as outlined in Scheme 1 using modified procedures available from the literature.[49,50] The PNI-py ligand was prepared by refluxing 4-nitro-1,8-naphthalic anhydride with an excess of 4-amino-pyridine in toluene containing triethylamine for 3 days at 120 °C to generate the 4-pyridyl-4-nitro-1,8-naphthalimide (NNI-py) intermediate. The isolated NNI-py species was then refluxed with an excess of piperidine in DMF for 2 h at 170 °C to obtain the pure final product, PNI-py, in 84% yield. The Re(I) complexes were prepared by departing from the analogous Re(N^N)$(CO)_3Cl$[51] precursor that was treated with 1.02 equiv of $AgBF_4$ for 3 h in acetonitrile at 85 °C shielded from light. The reaction solution was filtered through Celite and the residue washed with acetonitrile. The acetonitrile filtrate was removed via rotary evaporation, and the ancillary ligand of choice was added in a 1.2 equiv amount (PNI-py) or in large excess (4-etpy) and refluxed for 24 h at 85 °C in chloroform. Once isolated, the final product underwent a metathesis precipitation reaction to exchange the BF_4^- anion for the BF_6^- anion using NH_4PF_6 (concentrated NH_4PF_6 solution added to a 1/1 methanol/acetone mixture). The isolated molecules were then recrystallized as necessary in dichloromethane and hexanes to obtain each product in

https://dx.doi.org/10.1021/acs.inorgchem.0c00644
Inorg. Chem. 2020, 59, 8259−8271

acceptable yield. The final products (**Re1−5** and **Mod1−5**) were characterized using ^{1}H NMR spectroscopy, high-resolution electrospray mass spectrometry, elemental analysis, ATR-FTIR, and electrochemistry (**Mod1−5** only) (Figures S3−S23 and Table S1). These molecules are all thermally and photochemically stable in a range of organic solvents and in the solid state.

Electronic Structure Calculations. Density function theory (DFT) calculations at the M06//Def2-SVP/SDD level of theory in THF (PCM) were performed on all molecules in this study to obtain the geometry-optimized ground state (S_0) (Table S2). For **Mod1−5**, the HOMO consisted of primarily d orbitals and the LUMO consisted of primarily diimine π^* antibonding orbitals (Figures 3 and S24). **Re1−5** have a HOMO that consists of a π-bonding interaction on the PNI-py ligand in which the electron density resides over the naphthalimide and piperidine units. The LUMO consists of diimine π^* antibonding orbitals, and the LUMO+1 (LUMO+2 for **Re1**) consists of a π^* antibonding interaction localized on the PNI-py ligand, where the electron density migrates away from the piperidine and localizes more extensively on the naphthalimide subunit (Figures 3 and S25, and S26). Time-dependent DFT (TD-DFT) calculations at the same level of theory were performed to demonstrate which electronic transitions occurred upon ∼400 nm excitation (Table S3). All model complexes exhibited intense MLCT ($d\pi$(Re) → π^*(N^N)) transitions resulting from HOMO to LUMO excitation except for **Mod5**, in which the most intense transition was HOMO-1 to LUMO. The electron density in the HOMO resides primarily on the t_{2g} orbitals of the Re(I) center with little contribution from the pyridine ring and the electron density resides on the diimine ligand in the LUMO in **Mod1−5** (Figure 3). The HOMOs of **Re1−5** feature electron density centralized on the naphthalimide moiety in a bonding interaction. The LUMOs are centralized on the Re(I) $d\pi$ orbitals and the respective diimine ligand. The LUMO+1 is centralized on the naphthalimide in an antibonding interaction except for **Re1**, where the LUMO+1 has electron density on the π^*(phen) and LUMO+2 is similar to the LUMO+1 of **Re2−5**. The HOMOs located on the PNI-py ligand have identical energies in **Re1−5** (−6.55 ± 0.01 eV), while the corresponding LUMO+1 (LUMO+2 in **Re1**) energies are also the same (−2.74 ± 0.01 eV). The energies of the LUMOs (electron density on the diimine ligand) in **Mod1−5** are comparable to the energies of the LUMOs (electron density of the diimine ligand) calculated in **Re1−5** (Table S4). These combined data illustrate that the MLCT transition ($d\pi$(Re) → π^*(N^N)) energy remains the same irrespective of the nature of the ancillary ligand, indicating that there is no major change in the electronic transitions between **Mod1−5** and **Re1−5**. Triplet spin density calculations also aided in the determination of the lowest excited state configuration in all molecules (Figure S27). In **Mod1−5**, the triplet spin character was indicative of a ^{3}MLCT* ($d\pi$(Re) → π^*(N^N)) excited state, as the spin density was distributed over the Re atom and diimine ligands. For **Re1−3**, the triplet spin density rested entirely within the PNI-py ligand, **Re4** had triplet spin density on the Re atom and the deeb and PNI-py ligand fragments, and **Re5** had triplet spin resembling that of **Mod5**, in which it resides on the Re atom and biq ligand.

Static Absorption and Photoluminescence Spectroscopy. The PNI-py chromophore used in this study is similar to another naphthalimide, PNI-tol, which has been extensively studied, where they differ only in the substituent on the imide nitrogen (pyridine and toluene, respectively).[4,15,28,32,33,37] The combination of the absorption spectra of the Re(I) MLCT model chromophores (**Mod1−5**) in concert with PNI-py effectively reproduces the authentic electronic spectra of the Re(I) bichromophores **Re1−5** (Figure S28). This indicates that the addition of the PNI subunit to the pyridine bound to the Re(I) CDI core does not significantly alter the electronics of the resultant complexes. During preliminary photoluminescence studies, it was evident that the free PNI-py ligand interacted with the THF solvent, requiring us to identify an alternative model chromophore for the free ligand. Therefore, PNI was used as a free ligand surrogate due to their similar photophysical characteristics.[37,52]

The UV−vis absorption spectra were collected in aerated THF, and the corresponding photoluminescence spectra were measured in deaerated THF. The steady-state absorption and photoluminescence spectra for **Mod1−5** and **Re1−5** are presented in Figures 4 and 5, respectively. Additional

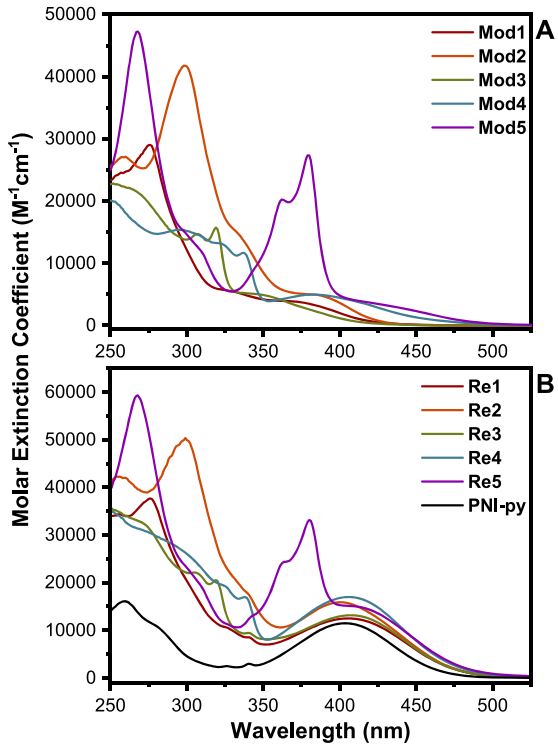

Figure 4. (A) Electronic absorption spectra of **Mod1−5** recorded in THF. (B) Electronic absorption spectra of **Re1−5** and PNI-py recorded in THF.

spectroscopic results are summarized in Table 1. The lowest energy absorption bands of **Mod1−5** (Figure 4a) are assigned to MLCT transitions, analogous to related molecules.[12,13,53−55] The higher energy absorption bands (>350 nm) of **Mod1−5** and **Re1−5** are assigned to the $\pi \rightarrow \pi^*$ transitions localized in the respective diimine ligand. The photoluminescence emission bands measured in **Mod1−5** (Figure 5a) are assigned to ^{3}MLCT-based PL due to their overall broad and featureless shape, large Stokes shift, and excited-state lifetimes (discussed below), all being characteristic of ^{3}MLCT phosphorescence (Figure 5a). Additionally, molecules of similar structure have also been assigned as to having ^{3}MLCT photoluminescence.[12,13,53,54] However, the unusual photoluminescence,

https://dx.doi.org/10.1021/acs.inorgchem.0c00644
Inorg. Chem. 2020, 59, 8259−8271

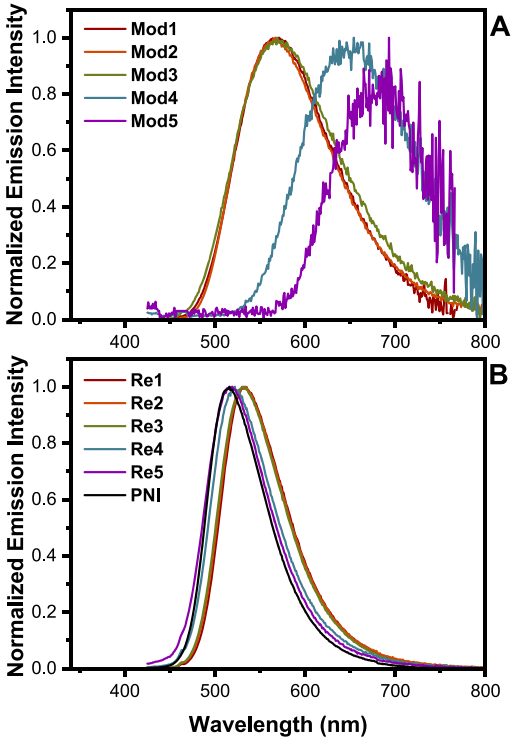

Figure 5. Static photoluminescence spectra of (A) **Mod1−5** and (B) **Re1−5** and PNI measured in deaerated THF on excitation at 408 nm.

Table 1. Steady-State Photophysical Data of Mod1−5, PNI-py, PNI, and Re1−5

	$\lambda_{abs\,max}$, nm (ε, M^{-1} cm^{-1})[a]	$\lambda_{em\,max}$, nm	Φ_{em}[d]	EnT, %[e]	$^3E_{em}$, cm^{-1}[f]
Mod1	364 (3950)	567	0.24		19500
Mod2	377 (5000)	567	0.27		20000
Mod3	339 (5000)	569	0.093		19900
Mod4	385 (5000)	650	0.013		16200
Mod5	407 (4200)	689	0.0024		14900
PNI	403 (11500)[b]	516[c]	0.80[c]		16200[g]
Re1	407 (12500)	533	0.13	84	
Re2	400 (15900)	536	0.091	89	
Re3	407 (13200)	533	0.18	78	
Re4	406 (15400)	525	0.049	94	
Re5	403 (15200)	516	0.061	92	

[a]Peak maximum given is of the lowest energy band (shoulder for **Mod1−5**). [b]Peak maximum and molar extinction coefficient used are for PNI-py. [c]Fluorescence data are for PNI. [d]Quantum yields of **Mod1−5** and PNI was measured using $[Ru(bpy)_3](PF_6)_2$ as the standard.[62] Quantum yields of **Re1−5** were measured using $[Ru(bpy)_3](PF_6)_2$ as the standard as well as PNI in toluene.[37,62] Samples for quantum yield studies were prepared at 0.1 OD at 408 nm (excitation) and were deaerated using the freeze−pump−thaw method with a 10% error. [e]EnT efficiency was calculated using eq 1. [f]Triplet energies were estimated from the emission profiles of **Mod1−5** and taking the tangent on the high-energy side of the band. [g]The triplet energy of PNI-py was obtained from sensitizing the triplet excited state by using 10% ethyl iodide as an additive and obtaining the phosphorescence spectrum of PNI-py at 77 K in a 2-MeTHF glass.

where the observed emission bands are coincident with **Mod1−3**, warranted further investigation as to whether the lowest excited state of **Mod1−3** is indeed of ^{3}MLCT character. Since the excited-state lifetime and nanosecond transient absorption spectra (discussed below) of **Mod3** were consistent with the photophysical properties expected from an MLCT transition, further investigation was needed for **Mod1** and **Mod2**. Electronic structure calculations suggested (discussed above) that the absorption transition arises from primarily dπ(Re) and π^*(phen/bcp) orbitals. Triplet spin density modeling of **Mod1** and **Mod2** predicts that the spin density resides on the dπ(Re) and the π^* orbitals of the diimine ligand present, suggesting that the transition is almost exclusively MLCT in nature. Moreover, there is literature precedence concerning the mixing of MLCT and LC transitions in Re-CDI molecules.[56−60] Furthermore, recent studies from our group on a similar Re-CDI containing 1,10-phenanthroline (phen) have shown that, when a stronger field ligand was incorporated as the ancillary ligand, the π^* orbitals of the phen moiety readily mixed with the dπ(Re) state. This mixing results in the lowest excited state being composed of LC and MLCT character, which markedly increased the excited state lifetime.[5] In a related study, we constructed a Re-CDI with phen and dimethylaminopyridine (dmap). This molecule possessed significant MLCT character in its lowest excited state[12] and was effectively used as a model for the bichromophores in that study despite there being some ^{3}LC contributions.[31] Therefore, we decided to use **Mod1** and **Mod2** as MLCT model molecules for comparison to their respective bichromophores, despite these complexes presenting a negligible amount of LC character, in subsequent sections of this paper, as the lowest excited states of **Mod1** and **Mod2** display predominantly MLCT character. The emission bands of **Mod4** and **Mod5** are red-shifted with respect to **Mod3** (Figure 5a), consistent with the bathochromic shift observed in their respective electronic absorption spectra in Figure 4a.

The lowest energy absorption band of **Re1−5** is primarily composed of the intraligand CT band from PNI-py (Figure 4b). The addition of the PNI-py chromophore does not completely obscure the MLCT transition observed in the model complexes and instead adds to the molar absorptivity of that wavelength region. Due to the overlap of the PNI-py localized absorptions with those of the MLCT transitions, excitation of the low-energy band does not selectively excite the PNI-py ligand exclusively; however, PNI-py absorbs the majority of the excitation light due to its significantly higher molar extinction coefficient in comparison to that of the MLCT transitions (Table 1).

In the photoluminescence spectra of **Re1−5** (Figure 5b), it is evident that the prevailing emission originates largely from the PNI moiety, analogous to the characteristic fluorescence observed in PNI itself, which is the black line displayed in Figure 5b. Therefore, the emission spectra measured in **Re1−5** (Figure 5b) is assigned as singlet ^{1}PNI fluorescence. Incidentally, these experimental observations are largely a consequence of the nature of the experiment, wherein low-energy excitation primarily promotes the ^{1}PNI-py ligand-centered excited state. Since there is incomplete energy transfer (discussed immediately below) occurring between the PNI-py ligand and the Re-CDI unit (Table 1) and only the brightest and fastest emission events are easily measured in static photoluminescence spectroscopy, all other lower-yielding light emission processes are effectively masked. However, some of the fluorescence of the PNI ligand is quenched (Table 1), suggesting that energy transfer is occurring via the FRET mechanism. The efficiency of the energy transfer processes occurring through FRET was calculated using eq 1, where

https://dx.doi.org/10.1021/acs.inorgchem.0c00644
Inorg. Chem. 2020, 59, 8259−8271

QY_{ReX} and QY_{PNI} denote the quantum yields measured for the PNI-py fluorescence emanating from **Re1−5** and PNI, respectively.[61]

$$EnT = 1 - \frac{QY_{ReX}}{QY_{PNI}} \quad (1)$$

The most efficient Förster energy transfer was measured in **Re4** at 94% and all of the **Re1−5** bichromophores featured FRET values >78% (Table 1). The residual fluorescence from the PNI-py subunit in **Re4** was sufficient to conceal all other emission events from the MLCT ($d\pi(Re) \rightarrow \pi^*(N^\wedge N)$) excited state that was observed in **Mod1−5** (Figure 5a). In $Re(PNI\text{-}phen)(CO)_3Cl$, where the PNI subunit was covalently linked to the diimine subunit, the FRET efficiency was greater than 99% and photoluminescence was observed from both the ^{1}PNI and ^{3}MLCT excited states in static PL experiments.[4] Clearly, the relocation of the PNI subunit to the tail end of the ancillary pyridine ligand in the present investigation significantly impacted the efficiency of the distance-dependent FRET processes in **Re1−5**.

Using the photoluminescence emission spectra of **Mod1−5**, the energies of the corresponding triplet excited states can be readily estimated. As expected, the three complexes that coincide, **Mod1−3**, have nearly identical triplet energies (~20000 cm^{-1}) and the two red-shifted molecules, **Mod4** (16200 cm^{-1}) and **Mod5** (14900 cm^{-1}), have significantly lower energies. The triplet energy of PNI-py (16200 cm^{-1}) was obtained from triplet sensitization of the free ligand at 77 K using 10% ethyl iodide in 2-MeTHF (Figure S29). A summary of the triplet-state energies of **Mod1−5** and PNI-py are collected in Table 1. The triplet states in the **Mod1−5** are assumed to correspond to the triplet energies of the ^{3}MLCT ($(d\pi(Re) \rightarrow \pi^*(N^\wedge N))$ excited state levels in **Re1−5**. The triplet energy of PNI-py recorded at 77 K in the presence of ethyl iodide is assumed to appropriately estimate the triplet energy of the PNI subunit. Given this combined experimental information, we can readily approximate the energy gap between the two chromophoric units in the **Re1−5** title molecules.

Nanosecond Transient Absorption Spectroscopy. Upon excitation using 355 nm nanosecond laser pulses (5 ns fwhm), **Mod1−5** (Figure S30) in deaerated THF display positive absorption features across the entire visible region. The excited-state features ranging between 350 and 400 nm are somewhat distorted due to overlap with the high molar absorptivity ground-state absorptions in this region. **Mod5** (Figures S30) features a structureless bleaching signal below 400 nm. **Mod3** and **Mod4** exhibited transient excited-state absorption features consistent with the ^{3}MLCT excited state, being comparable to the respective radical anion of the diimine unit resident in the structure (Figure S30). Single-wavelength kinetic analysis of these transient features yielded excited-state lifetimes consistent with ^{3}MLCT excited states: 301 and 65.1 ns for **Mod3** and **Mod4**, respectively (Table 2 and Figures S34 and S35).[63] **Mod5** and **Re5** featured similar excited-state spectral features that corresponded to the same excited-state lifetime, 38.9 and 39.5 ns for **Mod5** and **Re5**, respectively (Table 2, Figure 6, and Figures S30, S36, and S47). **Mod1** and **Mod2** possess excited-state spectral features that are similar due to their shared phenanthroline core but feature extended lifetimes that do not suggest pure ^{3}MLCT* behavior: τ = 1.50 μs for **Mod1** and τ = 8.24 μs for **Mod2** (Table 2 and Figures S30, S32, and S33).

Table 2. Time-Resolved TA and PL Data Recorded for Mod1−Mod5 and Re1−Re5 in THF[a]

	τ_{TA}, ns	τ_{PL}, ns	τ_{TA}, μs[b]
Mod1	1500	1480	
Mod2	8240	7600	
Mod3	301	296	
Mod4	65.1	68.1	
Mod5	38.9	39.5	
Re1			5110
Re2			918
Re3			1170
Re4			1.17
Re5	39.5	9.97	

[a]All kinetics were measured using the LP 920 laser flash photolysis system (Edinburgh Instruments) with a Vibrant 355 Nd:YAG/OPO system (OPOTEK) for pulsed laser excitation for single-wavelength kinetics detection at peak excited-state features (410 nm, 2.0 mJ/pulse). Samples were deaerated using the freeze−pump−thaw method. [b]Lifetime at theoretical infinite dilution.

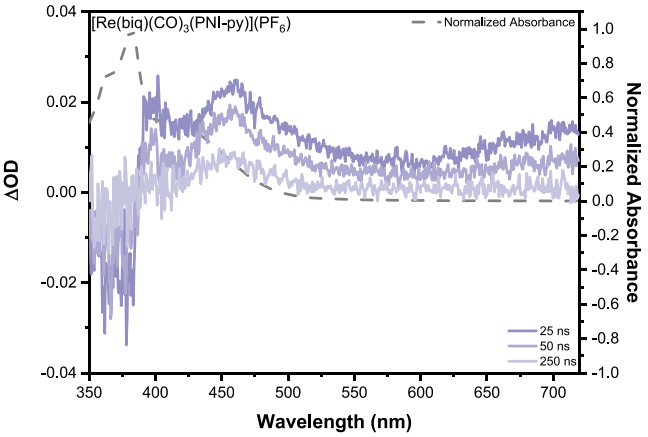

Figure 6. Transient absorption difference spectra with the corresponding ground-state absorption spectrum (dashed line) of **Re5** (45.4 μM) measured in THF with 355 nm laser pulses (5.0 mJ/pulse).

When **Re1−5** are excited with 355 nm light, the five Re(I) complexes fall under two distinguishing categories: (1) the TA difference spectra are indicative of the ^{3}PNI* excited state or (2) the TA difference spectra are qualitatively identical with those recorded for the respective model chromophores **Mod1−5**. **Re1−4** fall into category 1, whereas **Re5** falls into category 2. Beginning with **Re5** (Figure 6), it is safe to postulate that the lowest excited state is of ^{3}MLCT* ($d\pi(Re) \rightarrow \pi^*(biq)$) character. Evidence of this is clear-cut, as the profile of the transient absorption features are similar between **Re5** and **Mod5** (Figure 6 and Figure S30), and both have a ground-state bleach below 400 nm. Additionally, the lifetimes obtained from a single-wavelength analysis of the transient excited-state features of **Re5** (Figure S47) and **Mod 5** (Figure S36) are both single exponential, both equaling 40 ns, leaving little doubt that the nature of the excited state in both molecules is conserved.

In category 1, **Re1−3** have qualitatively identical TA difference spectra. There is a ground-state bleach centered near 400 nm and an excited-state absorption feature centered

https://dx.doi.org/10.1021/acs.inorgchem.0c00644
Inorg. Chem. 2020, 59, 8259−8271

at 465 nm (Figure 7a and Figures S37 and S38). **Re4** has an excited-state absorbance centered at 461 nm with a ground-state bleach located at 400 nm (Figure S39). These difference spectra are all consistent with ^{3}PNI*, as measured in previous studies.[4,32−34] One notable difference between the signal observed here and the signal observed in previous work is that there is not a second broad feature in the visible region spanning into the NIR. That second feature apparently results from the PNI moiety being covalently linked to the diimine ligand and is therefore absent in the current investigation. Another clear indicator that we are populating the ^{3}PNI* excited state in **Re1−4** are the biexponential, concentration-dependent lifetimes,[4,32,33] which are, in general, a characteristic of triplet naphthalimides.[64−66] This biexponential behavior is due to ^{3}PNI* self-quenching and was quantified by measuring the excited-state decay kinetics as a function of concentration, which yielded the theoretical lifetimes at infinite dilution (lifetime in the absence of self-quenching): τ_∞= 5110 μs in **Re1**, τ_∞= 918 μs in **Re2**, τ_∞= 1170 μs in **Re3**, and τ_∞= 1.17 μs in **Re4** (Figure 7b, Figures S44−S46, and Table 2), all of which are significantly longer than those of their respective model complexes.

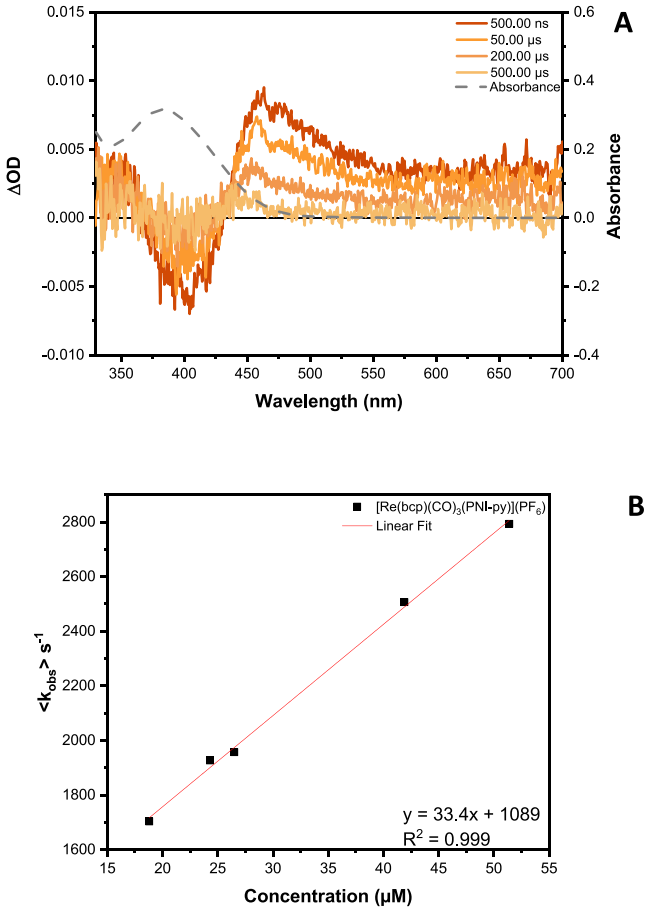

Figure 7. (A) Transient absorption difference spectra with the corresponding ground-state absorption spectrum (dashed line) of **Re2** (44.3 μM) recorded in THF with 355 nm laser pulses (5.0 mJ/pulse). (B) Concentration dependence study of **Re2** illustrating self-quenching behavior with single-wavelength transient absorption kinetics detected at 465 nm (λ_{ex} = 410 nm, 2.0 mJ/pulse). Samples were deaerated using the freeze−pump−thaw method.

Femtosecond Transient Absorption Spectroscopy. The ultrafast excited-state absorption difference spectra of **Mod1−5** are presented in Figure S48, while those of **Re2** and **Re5** are shown in Figures 8 and 9, respectively (λ_{ex} = 400 nm, 105 fs fwhm, 0.3 μJ/pulse); the corresponding data for **Re1**, **Re3**, and **Re4** are provided in Figures S54−S56. In **Mod1−4**, the positive transient absorption features are indicative of MLCT excited state absorptions that dominate across the visible region.[63,67] **Mod5** displays a ground-state bleach between 350 and 400 nm, coinciding with its ground-state absorption spectrum (Figure 4a). Across the visible and extending into the NIR spectral region, only excited-state absorptions are present in each of these molecules (Figure S48). **Re1−4** display stimulated emission peaks centered near 550 nm over the initial delay times and have excited-state absorption features centered at 430 nm that evolve over the time course of the experiment, eventually peaking at 460 nm (Figure 8 and Figures S54−S56). **Re5** (Figure 9) possesses

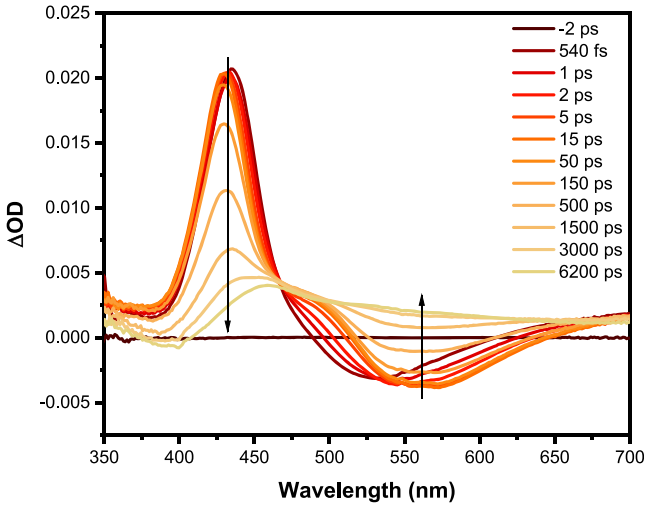

Figure 8. Excited-state absorption difference spectra of **Re2** in THF excited following 400 nm pulsed laser excitation (105 fs fwhm, 0.3 μJ/pulse).

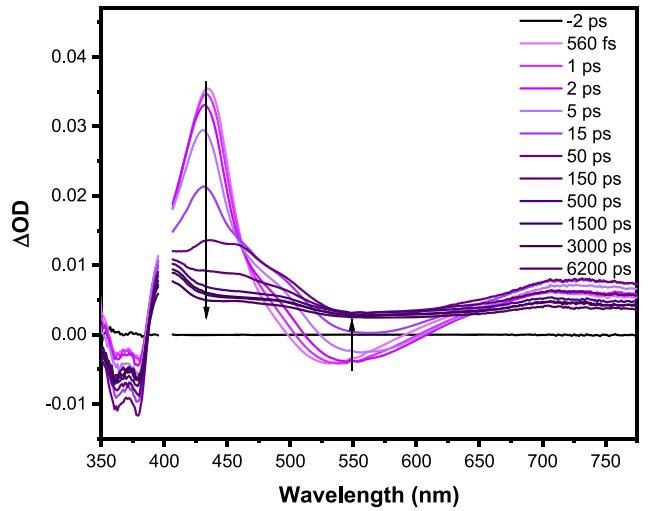

Figure 9. Excited state absorption difference spectra of **Re5** in THF excited following 400 nm pulsed laser excitation (105 fs fwhm, 0.3 μJ/pulse).

https://dx.doi.org/10.1021/acs.inorgchem.0c00644
Inorg. Chem. 2020, 59, 8259−8271

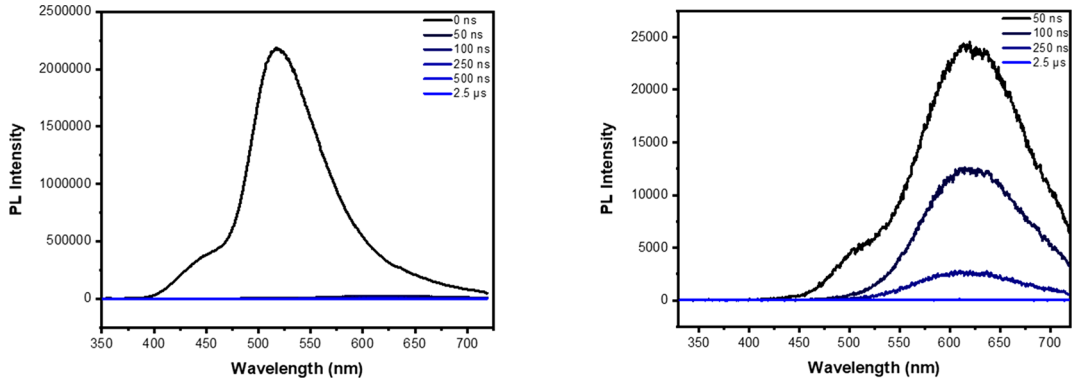

Figure 10. Representative (**Re1−4**) time-resolved photoluminescence data showing **Re4** early times (left) and delayed times (right) depicting the delayed phosphorescence from the ^{3}MLCT* excited state.

similar initial excited-state absorption features at 430 nm as well as a stimulated emission band near 550 nm. However, the 430 nm excited-state feature evolves into a structured absorption band with a peak centered at 400 nm and a shoulder near 500 nm extending into the NIR. There is also a ground-state bleach that echoes what was observed over the same wavelength region (350−400 nm) in **Mod5** (Figure S48).

All of the model complexes (**Mod1−5**) exhibit ultrafast excited-state absorption features and associated time constants (Figures S49−S53) that are significantly different from those of their PNI-containing counterparts (**Re1−5**). For **Mod1−3**, the fastest time constants recorded (τ = 120, 170, and 140 fs, respectively) arise from intersystem crossing and the formation of the radical anion on the diimine ligand. **Mod1−5** universally possessed a second time constant corresponding to vibrational relaxation (τ = 2.7 to 16 ps).[5,68] In addition to vibrational relaxation, **Mod4** and **Mod5** had an additional time constant on the order of hundreds of ps (τ = 107 and 120 ps). This slow time constant was also observed in the nanosecond time domain and, hence, is attributed to the onset of the triplet MLCT excited-state decay process. In **Mod1−5**, the line shape of the relaxed excited-state spectral feature persists into the nanosecond TA time scale, indicating that there are no additional excited states observed between the picosecond and nanosecond time domains.

The femtosecond transient absorption difference spectra of **Re1−Re4** (Figure 8 and Figures S54−S56) follow a similar energy migration trajectory, eventually resulting in ^{3}PNI* formation. Additionally, stimulated emission is present as a peak centered at 550 nm, as seen in previous papers for metal−organic chromophores containing a PNI subunit.[4,32,33] Over time, this feature red-shifts due to distortions caused by an overlap of excited-state features. Across all four molecules, immediately upon excitation at 400 nm, the signal that promptly appears corresponds to ^{1}PNI*, having a maximum at 430 nm. The ^{1}PNI* excited state decays, forming intermediate ^{1}MLCT* and ^{3}MLCT* states, eventually producing ^{3}PNI* over the course of 6 ns which has a peak maximum at 460 nm. **Re1−Re3** each exhibit three similar time constants (Figures S57−S59) following predominant excitation of ^{1}PNI*. The first decay component corresponds to the initial vibrational relaxation of "hot" ^{1}PNI* to form relaxed ^{1}PNI* (τ = 3.8, 2.1, and 3.5 ps for **Re1−Re3**, respectively). From ^{1}PNI*, the molecules undergo energy transfer through the FRET mechanism, preparing the ^{1}MLCT* state, which then immediately undergoes intersystem crossing (ISC) to the ^{3}MLCT* state (τ = 261, 260, and 256 ps for **Re1−Re3**, respectively). The FRET process (^{1}PNI* to ^{1}MLCT*) in the title molecules is occurring with much slower rate constants and lower efficiencies with respect to the related systems reported previously,[4,31] likely a consequence of the distance and orientation of the respective chromophores. Finally, the ^{3}MLCT* state engages in intramolecular triplet−triplet energy transfer (TTET) from the MLCT state on the rhenium complex to the PNI ligand having time constants of τ = 1.88, 1.79, and 2.3 ns for **Re1−Re3**, respectively. The corresponding time constant assigned to the intramolecular TTET process in **Re4** (Figure S60) is 701 ps, and at the present time we do not have a good explanation of why this time constant is significantly smaller than those measured in **Re1−Re3**. The remaining ultrafast processes in these molecules appear to be self-consistent. Vibrational relaxation of "hot" ^{1}PNI* followed by FRET to form the ^{1}MLCT* state and ISC to the ^{3}MLCT* state have time constants that are the same order of magnitude in **Re1−Re4** (2−4 ps for vibrational relaxation, 104−261 ps for FRET followed by ISC in **Re1−Re4**).

In stark contrast to **Re1−Re4**, **Re5** (Figure 9 and Figure S61) does not exhibit any evidence of ^{3}PNI* in its lowest excited state. However, evidence for ^{3}PNI* in the excited-state decay of **Re5** is clearly present during picosecond delay times. Additionally, the peak maximum of the "hot" ^{1}PNI* state in **Re5** is slightly red shifted (5 nm) due to the contributions of the ^{1}MLCT* (dπ(Re) → π*(biq)) state, in part believed to be a consequence of nonselective excitation. The time constant associated with this process is assigned to vibrational relaxation of "hot" ^{1}PNI* to ^{1}PNI* (τ = 9.6 ps). A potential explanation for the magnitude of this time constant is the greater contribution from the ^{1}MLCT* (dπ(Re) → π*(biq)) state, which is distinct with respect to the other molecules. The FRET and ISC processes in **Re5** ultimately lead to the ^{3}MLCT* (dπ(Re) → π*(biq, PNI)) state formation with a time constant of 76 ps, which persists throughout the duration of the experiment. **Re5** features the lowest ^{3}MLCT* excited state, distinct with respect to the remaining PNI-containing molecules, since the ^{3}MLCT* (dπ(Re) → π*(biq)) state energy is significantly lower than that of ^{3}PNI* (Table 1), thereby inhibiting any repopulation of the latter. This is also why the nanosecond transient absorption excited-state lifetime of **Re5** quantitatively matches that of **Mod5**, as they are both derived from a similar ^{3}MLCT excited-state configuration.

https://dx.doi.org/10.1021/acs.inorgchem.0c00644
Inorg. Chem. 2020, 59, 8259−8271

Excited-State Equilibrium. The decay kinetics of the ^{3}PNI* excited state absorption of **Re1−3** are similar, suggesting that the energy migrations between the bichromophores are comparable. Correlation between the excited-state absorption and delayed ^{3}MLCT* PL kinetics was not applicable to this study as in previous work[4] due to the unquenched fluorescence of the ^{1}PNI* moiety. Attempted collection of the red edge of the ^{3}MLCT* PL (655 nm) led to saturation of the detector even with the smallest possible slit widths. However, time-resolved PL data featured delayed phosphorescence from the ^{3}MLCT* (dπ(Re) → π*(N^N)) state (Figures S40−S42). Additionally, the lifetimes at infinite dilution (918−5110 μs, Table 2) of these molecules suggest that thermal equilibrium between the two triplet states occurs due to the lifetimes being intermediate between pure ^{3}MLCT* (dπ(Re) → π*(N^N)) (300 ns to 8 μs) and ^{3}PNI* (270 ms).[4] The lifetime is shortest in **Re2**, most likely since the ^{3}MLCT* (dπ(Re) → π*(bcp)) state is closest in energy to ^{3}PNI*, despite the PL data suggesting that all three complexes have virtually the same ^{3}MLCT* energy. The longer lifetimes are a consequence of the larger energy gaps between the two triplet states: i.e., the intramolecular rTTET process becomes less efficient with an increasing energy gap. **Re4** also displays evidence of thermal equilibrium as well through its lifetime at infinite dilution (1.17 μs) being intermediate between the ^{3}MLCT* (dπ(Re) → π*(deeb)) (70 ns) and ^{3}PNI* (270 ms). Time-resolved PL intensity decays also feature delayed ^{3}MLCT* (dπ(Re) → π*(deeb) PL (Figure 10). The decay of **Re4** being so much faster than **Re1−3** is likely a direct result of the triplet states in **Re4** having nearly isoenergetic levels, Table 1. Unlike **Re1−4**, **Re5** displays no evidence of thermal equilibrium between the ^{3}MLCT* (dπ(Re) → π*(biq) and ^{3}PNI* excited states. The lifetime of the excited-state absorption of **Re5** matches the lifetime of the excited-state absorption of **Mod5**, and there is no concrete evidence of delayed ^{3}MLCT* (dπ(Re) → π*(biq)) PL in this molecule (Figure S43).

Excited-State Evolution and Decay. The proposed energy level diagrams summarizing the energy migration pathways of **Re1−5** are presented in Figure 11 (for those of **Mod1−5**, see Figure S62). Upon initial excitation from the pump beam, **Re1−4** exhibit "ping-pong"-like energy transfer as seen in previous work.[4,31] In these molecules, the initial excited state is localized on the PNI (τ = 2.1−4.0 ps) unit, which then transfers to the ^{3}MLCT* (τ = 104−261 ps) and then finally back to the PNI unit (τ = 0.70−2.3 ns) in its triplet manifold. Due to the rapid rates for forward and reverse TTET in **Re1−Re4**, the composite excited-state lifetimes are dictated by the energy gap between the two triplet states in equilibrium: i.e., ^{3}MLCT and ^{3}PNI.

Re5 is the only bichromophore in this study that does not display a thermal equilibrium between the ^{3}MLCT (dπ(Re) → π*(biq)) and ^{3}PNI excited states. In the picosecond time domain, **Re5** promptly forms an excited state that is primarily localized on the PNI subunit (τ = 9.6 ps), which then transfers this energy to the ^{3}MLCT* (dπRe → π*(biq)) manifold (τ = 76 ps). However, there is also evidence of some population of the ^{3}PNI excited state on the same time scale. From this time point forward, the remaining excited state features decay most consistent with the ^{3}MLCT state returning to the ground state with a time constant of 40 ns, echoing the latter decay process occurring in **Mod5**.

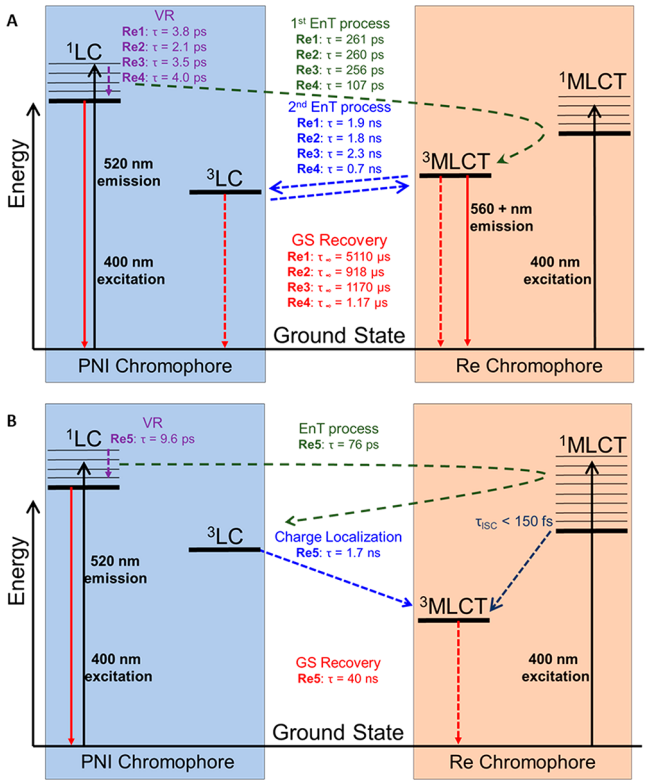

Figure 11. Qualitative energy level diagrams of the photophysical processes occurring in **Re1−4** (A) and **Re5** (B).

CONCLUSIONS

In this study, the excited-state processes and associated energetic pathways of a series of five Re(I)-PNI bichromophores have been elucidated using a combination of transient absorption spectroscopy, time-resolved PL spectroscopy, and electronic structure calculations. These bichromophoric molecules and their respective models were synthesized by preparing the parent Re-CDI moiety with a series of five diimine ligands and substituting PNI-py or 4-etpy into the ancillary position following reported procedures.[50] The unique diimine ligands yielded profound changes in the resultant molecular photophysical properties. On placement of the PNI subunit in an ancillary ligand position, the various energy transfer processes occurring between the relevant MLCT and PNI excited states were able to be quantitatively assessed. From the battery of static and time-resolved spectroscopic techniques utilized as described above, the data suggest that four of the five bichromophores in this study (**Re1−Re4**) display energetic pathways indicative of "ping-pong" energy transfer, as observed in previous work.[4,31] In **Re1−Re4**, the initially populated ^{1}PNI* excited state transfers energy to the Re(I) MLCT complex, producing the ^{3}MLCT* state, which thermally equilibrates with the ^{3}PNI* state. These four molecules decay to their ground states with lifetimes markedly exceeding those observed in their respective model MLCT chromophores, **Mod1−4**. **Re5**, which possesses the lowest energy MLCT excited state in the series, is initially populated through the ^{1}PNI* excited state, whose energy rapidly transfers to the MLCT manifold, although there is some evidence for ^{3}PNI character as well. This molecule ultimately decays back to its ground state with a transient absorption determined excited-state lifetime equivalent to that of **Mod5**.

https://dx.doi.org/10.1021/acs.inorgchem.0c00644
Inorg. Chem. 2020, 59, 8259−8271

■ ASSOCIATED CONTENT

Supporting Information

The Supporting Information is available free of charge at https://pubs.acs.org/doi/10.1021/acs.inorgchem.0c00644.

Synthetic details, structural characterization data, additional static and time-resolved spectra, and density functional theory calculations for the molecules in this study (PDF)

■ AUTHOR INFORMATION

Corresponding Author

Felix N. Castellano − *Department of Chemistry, North Carolina State University, Raleigh, North Carolina 27695-8204, United States;* orcid.org/0000-0001-7546-8618; Phone: (919) 515-3021; Email: fncastel@ncsu.edu

Authors

Kaylee A. Wells − *Department of Chemistry, North Carolina State University, Raleigh, North Carolina 27695-8204, United States;* orcid.org/0000-0002-6870-6574

James E. Yarnell − *Department of Chemistry, North Carolina State University, Raleigh, North Carolina 27695-8204, United States; Department of Chemistry & Chemistry Research Center, United States Air Force Academy, Colorado Springs, Colorado 80840-6230, United States*

Jonathan R. Palmer − *Department of Chemistry, North Carolina State University, Raleigh, North Carolina 27695-8204, United States*

Tia S. Lee − *Department of Chemistry, North Carolina State University, Raleigh, North Carolina 27695-8204, United States;* orcid.org/0000-0003-0635-6668

Christopher M. Papa − *Department of Chemistry, North Carolina State University, Raleigh, North Carolina 27695-8204, United States*

Complete contact information is available at: https://pubs.acs.org/10.1021/acs.inorgchem.0c00644

Author Contributions

The manuscript was written through contributions of all authors. All authors have given approval to the final version of the manuscript.

Notes

The authors declare no competing financial interest.

■ ACKNOWLEDGMENTS

This work was supported by the U.S. Department of Energy, Office of Science, Office of Basic Energy Sciences, under Award No. DE-SC0011979. Some personnel were supported by the National Science Foundation (CHE-1665033, K.A.W.), the Air Force Institute of Technology (AFIT, J.E.Y.), and the Air Force Office of Scientific Research (FA9550-18-1-0331, T.S.L.).

■ REFERENCES

(1) Wrighton, M.; Morse, D. L. Nature of the lowest excited state in tricarbonylchloro-1,10-phenanthrolinerhenium(I) and related complexes. *J. Am. Chem. Soc.* **1974**, *96*, 998−1003.

(2) Vlček, A. Ultrafast Excited-State Processes in Re(I) Carbonyl-Diimine Complexes: From Excitation to Photochemistry. In *Photophysics of Organometallics*; Lees, A. J., Ed.; Springer Berlin Heidelberg: Berlin, Heidelberg, 2010; pp 115−158.

(3) Kumar, A.; Sun, S.-S.; Lees, A. J. Photophysics and Photochemistry of Organometallic Rhenium Diimine Complexes. In *Photophysics of Organometallics*; Lees, A. J., Ed.; Springer Berlin Heidelberg: Berlin, Heidelberg, 2010; pp 37−71.

(4) Yarnell, J. E.; Deaton, J. C.; McCusker, C. E.; Castellano, F. N. Bidirectional "Ping-Pong" Energy Transfer and 3000-Fold Lifetime Enhancement in a Re(I) Charge Transfer Complex. *Inorg. Chem.* **2011**, *50*, 7820−7830.

(5) Favale, J. M.; Danilov, E. O.; Yarnell, J. E.; Castellano, F. N. Photophysical Processes in Rhenium(I) Diiminetricarbonyl Arylisocyanides Featuring Three Interacting Triplet Excited States. *Inorg. Chem.* **2019**, *58*, 8750−8762.

(6) Patrocínio, A. O. T.; Murakami Iha, N. Y. Photoswitches and Luminescent Rigidity Sensors Based on fac-$[Re(CO)_3(Me_4\ phen)(L)]^+$. *Inorg. Chem.* **2008**, *47*, 10851−10857.

(7) Schanze, K. S.; Brent Macqueen, D.; Perkins, T. A.; Cabana, L. A. Studies of intramolecular electron and energy transfer using the *fac*-(diimine)ReI$(CO)_3$ chromophore. *Coord. Chem. Rev.* **1993**, *122*, 63−89.

(8) Lo, K. K.-W. Exploitation of Luminescent Organometallic Rhenium(I) and Iridium(III) Complexes in Biological Studies. In *Photophysics of Organometallics*; Lees, A. J., Ed.; Springer Berlin Heidelberg: Berlin, Heidelberg, 2010; pp 73−114.

(9) Chakraborty, I.; Jimenez, J.; Sameera, W. M. C.; Kato, M.; Mascharak, P. K. Luminescent Re(I) Carbonyl Complexes as Trackable PhotoCORMs for CO delivery to Cellular Targets. *Inorg. Chem.* **2017**, *56*, 2863−2873.

(10) Kuramochi, Y.; Fujisawa, Y.; Satake, A. Photocatalytic CO_2 Reduction Mediated by Electron Transfer via the Excited Triplet State of Zn(II) Porphyrin. *J. Am. Chem. Soc.* **2020**, *142*, 705−709.

(11) Bruch, Q. J.; Connor, G. P.; Chen, C.-H.; Holland, P. L.; Mayer, J. M.; Hasanayn, F.; Miller, A. J. M. Dinitrogen Reduction to Ammonium at Rhenium Utilizing Light and Proton-Coupled Electron Transfer. *J. Am. Chem. Soc.* **2019**, *141*, 20198−20208.

(12) Caspar, J. V.; Meyer, T. J. Application of the energy gap law to nonradiative, excited-state decay. *J. Phys. Chem.* **1983**, *87*, 952−957.

(13) Sacksteder, L.; Zipp, A. P.; Brown, E. A.; Streich, J.; Demas, J. N.; DeGraff, B. A. Luminescence studies of pyridine α-diimine rhenium(I) tricarbonyl complexes. *Inorg. Chem.* **1990**, *29*, 4335−4340.

(14) Lavie-Cambot, A.; Lincheneau, C.; Cantuel, M.; Leydet, Y.; McClenaghan, N. D. Reversible electronic energy transfer: a means to govern excited-state properties of supramolecular systems. *Chem. Soc. Rev.* **2010**, *39*, 506−515.

(15) Franco, F.; Cometto, C.; Garino, C.; Minero, C.; Sordello, F.; Nervi, C.; Gobetto, R. Photo- and Electrocatalytic Reduction of CO_2 by $[Re(CO)_3\{\alpha,\alpha'$-Diimine-(4-piperidinyl-1,8-naphthalimide)$\}Cl]$ Complexes. *Eur. J. Inorg. Chem.* **2015**, *2015*, 296−304.

(16) Lainé, P. P.; Bedioui, F.; Loiseau, F.; Chiorboli, C.; Campagna, S. Conformationally Gated Photoinduced Processes within Photosensitizer Acceptor Dyads Based on Osmium(II) Complexes with Triarylpyridinio-Functionalized Terpyridyl Ligands: Insights from Experimental Study. *J. Am. Chem. Soc.* **2006**, *128*, 7510−7521.

(17) Leydet, Y.; Bassani, D. M.; Jonusauskas, G.; McClenaghan, N. D. Equilibration between Three Different Excited States in a Bichromophoric Copper(I) Polypyridine Complex. *J. Am. Chem. Soc.* **2007**, *129*, 8688−8689.

(18) Cohen, B. W.; Lovaasen, B. M.; Simpson, C. K.; Cummings, S. D.; Dallinger, R. F.; Hopkins, M. D. 1000-Fold Enhancement of Luminescence Lifetimes via Energy-Transfer Equilibration with the T1 State of Zn(TPP). *Inorg. Chem.* **2010**, *49*, 5777−5779.

(19) Wilson, G. J.; Launikonis, A.; Sasse, W. H. F.; Mau, A. W. H. Excited-State Processes in Ruthenium(II) Bipyridine Complexes Containing Covalently Bound Arenes. *J. Phys. Chem. A* **1997**, *101*, 4860−4866.

(20) Wilson, G. J.; Launikonis, A.; Sasse, W. H. F.; Mau, A. W. H. Chromophore-Specific Quenching of Ruthenium Trisbipyridine-Arene Bichromophores by Methyl Viologen. *J. Phys. Chem. A* **1998**, *102*, 5150−5156.

(21) Michalec, J. F.; Bejune, S. A.; McMillin, D. R. Multiple Ligand-Based Emissions from a Platinum(II) Terpyridine Complex Attached to Pyrene. *Inorg. Chem.* **2000**, *39*, 2708−2709.
(22) McClenaghan, N. D.; Barigelletti, F.; Maubert, B.; Campagna, S. Towards ruthenium(II) polypyridine complexes with prolonged and predetermined excited state lifetimes. *Chem. Commun.* **2002**, 602−603.
(23) Passalacqua, R.; Loiseau, F.; Campagna, S.; Fang, Y.-Q.; Hanan, G. S. In Search of Ruthenium(II) Complexes Based on Tridentate Polypyridine Ligands that Feature Long-lived Room-Temperature Luminescence: The Multichromophore Approach. *Angew. Chem., Int. Ed.* **2003**, *42*, 1608−1611.
(24) Whited, M. T.; Djurovich, P. I.; Roberts, S. T.; Durrell, A. C.; Schlenker, C. W.; Bradforth, S. E.; Thompson, M. E. Singlet and Triplet Excitation Management in a Bichromophoric Near-Infrared-Phosphorescent BODIPY-Benzoporphyrin Platinum Complex. *J. Am. Chem. Soc.* **2011**, *133*, 88−96.
(25) Simon, J. A.; Curry, S. L.; Schmehl, R. H.; Schatz, T. R.; Piotrowiak, P.; Jin, X.; Thummel, R. P. Intramolecular Electronic Energy Transfer in Ruthenium(II) Diimine Donor/Pyrene Acceptor Complexes Linked by a Single C-C Bond. *J. Am. Chem. Soc.* **1997**, *119*, 11012−11022.
(26) Tyson, D. S.; Castellano, F. N. Intramolecular Singlet and Triplet Energy Transfer in a Ruthenium(II) Diimine Complex Containing Multiple Pyrenyl Chromophores. *J. Phys. Chem. A* **1999**, *103*, 10955−10960.
(27) Castellano, F. N. Altering Molecular Photophysics by Merging Organic and Inorganic Chromophores. *Acc. Chem. Res.* **2015**, *48*, 828−839.
(28) Castellano, F. N. Transition metal complexes meet the rylenes. *Dalton Trans.* **2012**, *41*, 8493.
(29) Tyson, D. S.; Bialecki, J.; Castellano, F. N. Ruthenium(II) complex with a notably long excited state lifetime. *Chem. Commun.* **2000**, 2355−2356.
(30) Tyson, D. S.; Henbest, K. B.; Bialecki, J.; Castellano, F. N. Excited State Processes in Ruthenium(II)/Pyrenyl Complexes Displaying Extended Lifetimes. *J. Phys. Chem. A* **2001**, *105*, 8154−8161.
(31) Yarnell, J. E.; Wells, K. A.; Palmer, J. R.; Breaux, J. M.; Castellano, F. N. Excited-State Triplet Equilibria in a Series of Re(I)-Naphthalimide Bichromophores. *J. Phys. Chem. B* **2019**, *123*, 7611−7627.
(32) Yarnell, J. E.; McCusker, C. E.; Leeds, A. J.; Breaux, J. M.; Castellano, F. N. Exposing the Excited-State Equilibrium in an Ir(III) Bichromophore: A Combined Time Resolved Spectroscopy and Computational Study. *Eur. J. Inorg. Chem.* **2016**, *2016*, 1808−1818.
(33) Tyson, D. S.; Luman, C. R.; Zhou, X.; Castellano, F. N. New Ru(II) Chromophores with Extended Excited-State Lifetimes. *Inorg. Chem.* **2001**, *40*, 4063−4071.
(34) McCusker, C. E.; Chakraborty, A.; Castellano, F. N. Excited State Equilibrium Induced Lifetime Extension in a Dinuclear Platinum(II) Complex. *J. Phys. Chem. A* **2014**, *118*, 10391−10399.
(35) Chandrasekharam, M.; Srinivasarao, C.; Suresh, T.; Reddy, M. A.; Raghavender, M.; Rajkumar, G.; Srinivasu, M.; Reddy, P. Y. High spectral response heteroleptic ruthenium (II) complexes as sensitizers for dye sensitized solar cells. *J. Chem. Sci.* **2011**, *123*, 37−46.
(36) Suzuki, K.; Kobayashi, A.; Kaneko, S.; Takehira, K.; Yoshihara, T.; Ishida, H.; Shiina, Y.; Oishi, S.; Tobita, S. Reevaluation of absolute luminescence quantum yields of standard solutions using a spectrometer with an integrating sphere and a back-thinned CCD detector. *Phys. Chem. Chem. Phys.* **2009**, *11*, 9850−9860.
(37) Greenfield, S. R.; Svec, W. A.; Gosztola, D.; Wasielewski, M. R. Multistep Photochemical Charge Separation in Rod-like Molecules Based on Aromatic Imides and Diimides. *J. Am. Chem. Soc.* **1996**, *118*, 6767−6777.
(38) Garakyaraghi, S.; Danilov, E. O.; McCusker, C. E.; Castellano, F. N. Transient Absorption Dynamics of Sterically Congested Cu(I) MLCT Excited States. *J. Phys. Chem. A* **2015**, *119*, 3181−3193.
(39) Frisch, M. J.; Trucks, G. W.; Schlegel, H. B.; Scuseria, G. E.; Robb, M. A.; Cheeseman, J. R.; Scalmani, G.; Barone, V.; Petersson, G. A., et al. *Gaussian 16, Rev. A.03*; Gaussian Inc.: Wallingford, CT, 2016.
(40) Zhao, Y.; Truhlar, D. G. The M06 suite of density functionals for main group thermochemistry, thermochemical kinetics, noncovalent interactions, excited states, and transition elements: two new functionals and systematic testing of four M06-class functionals and 12 other functionals. *Theor. Chem. Acc.* **2008**, *120*, 215−241.
(41) Weigend, F.; Ahlrichs, R. Balanced basis sets of split valence, triple zeta valence and quadruple zeta valence quality for H to Rn: Design and assessment of accuracy. *Phys. Chem. Chem. Phys.* **2005**, *7*, 3297−3305.
(42) Andrae, D.; Häußermann, U.; Dolg, M.; Stoll, H.; Preuß, H. Energy-adjustedab initio pseudopotentials for the second and third row transition elements. *Theor. Chim. Acta* **1990**, *77*, 123−141.
(43) Ehlers, A. W.; Böhme, M.; Dapprich, S.; Gobbi, A.; Höllwarth, A.; Jonas, V.; Köhler, K. F.; Stegmann, R.; Veldkamp, A.; Frenking, G. A set of f-polarization functions for pseudo-potential basis sets of the transition metals Sc-Cu, Y-Ag and La-Au. *Chem. Phys. Lett.* **1993**, *208*, 111−114.
(44) Cossi, M.; Scalmani, G.; Rega, N.; Barone, V. New developments in the polarizable continuum model for quantum mechanical and classical calculations on molecules in solution. *J. Chem. Phys.* **2002**, *117*, 43.
(45) Dennington, R.; Keith, T. A.; Millam, J. M. *Gauss View, Ver, 6*; Semichem Inc.: Shawnee Mission, KS, 2016.
(46) Stratmann, R. E.; Scuseria, G. E.; Frisch, M. J. An efficient implementation of time-dependent density-functional theory for the calculation of excitation energies of large molecules. *J. Chem. Phys.* **1998**, *109*, 8218.
(47) Bauernschmitt, R.; Ahlrichs, R. Treatment of electronic excitations within the adiabatic approximation of time dependent density functional theory. *Chem. Phys. Lett.* **1996**, *256*, 454−464.
(48) Casida, M. E.; Jamorski, C.; Casida, K. C.; Salahub, D. R. Molecular excitation energies to high-lying bound states from time-dependent density-functional response theory: Characterization and correction of the time-dependent local density approximation ionization threshold. *J. Chem. Phys.* **1998**, *108*, 4439.
(49) Kitchen, J. A.; Martinho, P. N.; Morgan, G. G.; Gunnlaugsson, T. Synthesis, crystal structure and EPR spectroscopic analysis of novel copper complexes formed from N-pyridyl-4-nitro-1,8-naphthalimide ligands. *Dalton Trans.* **2014**, *43*, 6468.
(50) Langdon-Jones, E. E.; Williams, C. F.; Hayes, A. J.; Lloyd, D.; Coles, S. J.; Horton, P. N.; Groves, L. M.; Pope, S. J. A. Luminescent 1,8-Naphthalimide-Derived ReI Complexes: Syntheses, Spectroscopy, X-ray Structure and Preliminary Bioimaging in Fission Yeast Cells. *Eur. J. Inorg. Chem.* **2017**, *2017*, 5279−5287.
(51) Worl, L. A.; Duesing, R.; Chen, P.; Ciana, L. D.; Meyer, T. J. Photophysical properties of polypyridyl carbonyl complexes of rhenium(I). *J. Chem. Soc., Dalton Trans.* **1991**, 849.
(52) Kucheryavy, P.; Li, G.; Vyas, S.; Hadad, C.; Glusac, K. D. Electronic Properties of 4-Substituted Naphthalimides. *J. Phys. Chem. A* **2009**, *113*, 6453−6461.
(53) Zipp, A. P.; Sacksteder, L.; Streich, J.; Cook, A.; Demas, J. N.; Degraff, B. A. Luminescence of rhenium(I) complexes with highly sterically hindered α-diimine ligands. *Inorg. Chem.* **1993**, *32*, 5629−5632.
(54) Wallace, L.; Rillema, D. P. Photophysical properties of rhenium(I) tricarbonyl complexes containing alkyl- and aryl-substituted phenanthrolines as ligands. *Inorg. Chem.* **1993**, *32*, 3836−3843.
(55) Moya, S. A.; Guerrero, J.; Pastene, R.; Sartori, R.; Schmidt, R.; Sariego, R.; Sanz-Aparicio, J.; Fonseca, I.; Martinez-Ripoll, M. Metallic Carbonyl Complexes Containing Heterocycle Nitrogen Ligands. 2. Tricarbonylbromo(3,3′-R-2,2′-biquinoline)Rhenium(I) Compounds. *Inorg. Chem.* **1994**, *33*, 2341−2346.

https://dx.doi.org/10.1021/acs.inorgchem.0c00644
Inorg. Chem. 2020, 59, 8259−8271

(56) Striplin, D. R.; Crosby, G. A. Photophysical investigations of rhenium(I)$Cl(CO)_3$(phenanthroline) complexes. *Coord. Chem. Rev.* **2001**, *211*, 163−175.
(57) Striplin, D. R.; Crosby, G. A. Nature of the emitting 3MLCT manifold of rhenium(I)(diimine)$(CO)_3Cl$ complexes. *Chem. Phys. Lett.* **1994**, *221*, 426−430.
(58) Mai, S.; Gattuso, H.; Fumanal, M.; Muñoz-Losa, A.; Monari, A.; Daniel, C.; González, L. Excited-states of a rhenium carbonyl diimine complex: solvation models, spin−orbit coupling, and vibrational sampling effects. *Phys. Chem. Chem. Phys.* **2017**, *19*, 27240−27250.
(59) Yang, L.; Ren, A. M.; Feng, J. K.; Liu, X. J.; Ma, Y. G.; Zhang, M.; Liu, X. D.; Shen, J. C.; Zhang, H. X. Theoretical Studies of Ground and Excited Electronic States in a Series of Halide Rhenium(I) Bipyridine Complexes. *J. Phys. Chem. A* **2004**, *108*, 6797−6808.
(60) Vlček, A.; Záliš, S. Comments on "Theoretical Studies of Ground and Excited Electronic States in a Series of Halide Rhenium(I) Bipyridine Complexes. *J. Phys. Chem. A* **2005**, *109*, 2991−2992.
(61) Lakowicz, J. R. *Principles of Fluorescence Spectroscopy*, 3rd ed.; Springer Science+Business Media: New York, 2006.
(62) Suzuki, K.; Kobayashi, A.; Kaneko, S.; Takehira, K.; Yoshihara, T.; Ishida, H.; Shiina, Y.; Oishi, S.; Tobita, S. Reevaluation of absolute luminescence quantum yields of standard solutions using a spectrometer with an integrating sphere and a back-thinned CCD detector. *Phys. Chem. Chem. Phys.* **2009**, *11*, 9850.
(63) Kalyanasundaram, K. Luminescence and redox reactions of the metal-to-ligand charge-transfer excited state of tricarbonylchloro-(polypyridyl)rhenium(I) complexes. *J. Chem. Soc., Faraday Trans. 2* **1986**, *82*, 2401.
(64) Aveline, B. M.; Matsugo, S.; Redmond, R. W. Photochemical Mechanisms Responsible for the Versatile Application of Naphthalimides and Naphthaldiimides in Biological Systems. *J. Am. Chem. Soc.* **1997**, *119*, 11785−11795.
(65) Rogers, J. E.; Kelly, L. A. Nucleic Acid Oxidation Mediated by Naphthalene and Benzophenone Imide and Diimide Derivatives: Consequences for DNA Redox Chemistry. *J. Am. Chem. Soc.* **1999**, *121*, 3854−3861.
(66) Rogers, J. E.; Weiss, S. J.; Kelly, L. A. Photoprocesses of Naphthalene Imide and Diimide Derivatives in Aqueous Solutions of DNA. *J. Am. Chem. Soc.* **2000**, *122*, 427−436.
(67) El Nahhas, A.; Consani, C.; Blanco-RodríGuez, A. M. A.; Lancaster, K. M.; Braem, O.; Cannizzo, A.; Towrie, M.; Clark, I. P.; Záliš, S.; Chergui, M.; Vlček, A. N. Ultrafast Excited-State Dynamics of Rhenium(I) Photosensitizers $[Re(Cl)(CO)_3(N, N)]$ and $[Re(imidazole)(CO)_3(N, N)]^+$: Diimine Effects. *Inorg. Chem.* **2011**, *50*, 2932−2943.
(68) Liard, D. J.; Busby, M.; Matousek, P.; Towrie, M.; Vlček, A. Picosecond Relaxation of 3MLCT Excited States of $[Re(Etpy)(CO)_3(dmb)]^+$ and $[Re(Cl)(CO)_3(bpy)]$ as Revealed by Time-Resolved Resonance Raman, UV-vis, and IR Absorption Spectroscopy. *J. Phys. Chem. A* **2004**, *108*, 2363−2369.

https://dx.doi.org/10.1021/acs.inorgchem.0c00644
Inorg. Chem. 2020, 59, 8259−8271